THE JOURNAL OF PHYSICAL CHEMISTRY B

Article

pubs.acs.org/JPCB

Modelling Time-Resolved Two-Dimensional Electronic Spectroscopy of the Primary Photoisomerization Event in Rhodopsin

Ivan Rivalta,*[,†,‡] Artur Nenov,[‡] Oliver Weingart,[§] Giulio Cerullo,[∥] Marco Garavelli,*[,†,‡] and Shaul Mukamel*[,⊥]

[†]Université de Lyon, CNRS, Institut de Chimie de Lyon, École Normale Supérieure de Lyon, 46 Allée d'Italie, F-69364 Lyon Cedex 07, France

[‡]Dipartimento di Chimica "G. Ciamician", Università di Bologna, V. F. Selmi 2, 40126 Bologna, Italy

[§]Institut für Theoretische Chemie und Computerchemie, Heinrich-Heine-Universität Düsseldorf, Universitätsstr. 1, 40225 Düsseldorf, Germany

[∥]IFN-CNR, Dipartimento di Fisica, Politecnico di Milano, Piazza L. da Vinci 32, 20133 Milano, Italy

[⊥]Department of Chemistry, University of California, Irvine, California 92697-2025, United States

Supporting Information

ABSTRACT: Time-resolved two-dimensional (2D) electronic spectra (ES) tracking the evolution of the excited state manifolds of the retinal chromophore have been simulated along the photoisomerization pathway in bovine rhodopsin, using a state-of-the-art hybrid QM/MM approach based on multiconfigurational methods. Simulations of broadband 2D spectra provide a useful picture of the overall detectable 2D signals from the near-infrared (NIR) to the near-ultraviolet (UV). Evolution of the stimulated emission (SE) and excited state absorption (ESA) 2D signals indicates that the $S_1 \rightarrow S_N$ (with $N \geq 2$) ESAs feature a substantial blue-shift only after bond inversion and partial rotation along the *cis* → *trans* isomerization angle, while the SE rapidly red-shifts during the photoinduced skeletal relaxation of the polyene chain. Different combinations of pulse frequencies are proposed in order to follow the evolution of specific ESA signals. These include a *two-color* 2DVis/NIR setup especially suited for tracking the evolution of the $S_1 \rightarrow S_2$ transitions that can be used to discriminate between different photochemical mechanisms of retinal photoisomerization as a function of the environment. The reported results are consistent with the available time-resolved pump−probe experimental data, and may be used for the design of more elaborate transient 2D electronic spectroscopy techniques.

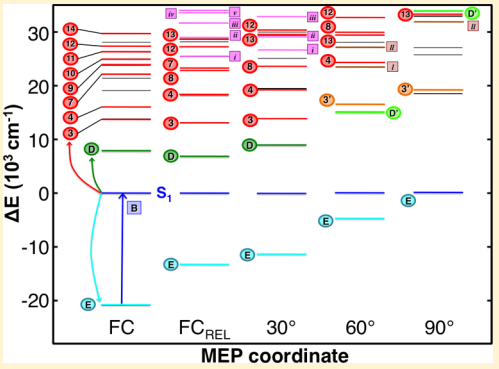

INTRODUCTION

Rhodopsin (Rh) is a type II opsin found in the photoreceptor rod cells of the retina, where it is used for night and peripheral vision. The chromophore responsible for light reception in Rh is the polyene 11-*cis*-retinal, which covalently binds the opsin apoprotein through a Schiff base (SB) linkage to the lysine residue Lys296, forming the 11-*cis*-retinal protonated Schiff base (PSB11) shown in Figure 1. Rh is the only type II opsin for which the X-ray structure has been resolved,[1−7] representing a paradigm system for fundamental studies of the primary event in vision and a reference model for the design of biomimetic photochromic devices.[8−10] Upon absorption of visible light (with an absorption maximum at ∼500 nm, i.e., at a frequency of ν_{max} = ∼20 000 cm^{-1}), PSB11 undergoes ultrafast (200 fs) 11-*cis* → all-*trans* isomerization (see Figure 1a), triggering protein conformational changes that initiate the signal transduction processes in vision.[11] Fundamental understanding of retinal chromophore photochemistry and disentanglement of environmental effects, such as the electrostatic effects of the embedding proteins or the surrounding solvent molecules, are crucial for the design of biomimetic photosensitive devices.

Extensive computational studies aimed to unravel environmental effects which tune the photophysical and photochemical properties of retinals have been recently reviewed,[12] indicating possible molecular mechanisms explaining the different behaviors of retinal photoisomerization in various surroundings. Different environmental conditions could, in fact, alter the intrinsic properties of the chromophore by modulating the interplay between the covalent excited states and the ionic "photoactive" S_1 state. It has been proposed that, according to the so-called *three-state* model, the covalent S_2 excited state is directly involved in slowing down the photoisomerization reaction in bacteriorhodopsin,[13,14] and likely also in solvated

Special Issue: James L. Skinner Festschrift

Received: March 13, 2014
Revised: May 2, 2014
Published: May 2, 2014

   dx.doi.org/10.1021/jp502538m | J. Phys. Chem. B 2014, 118, 8396−8405

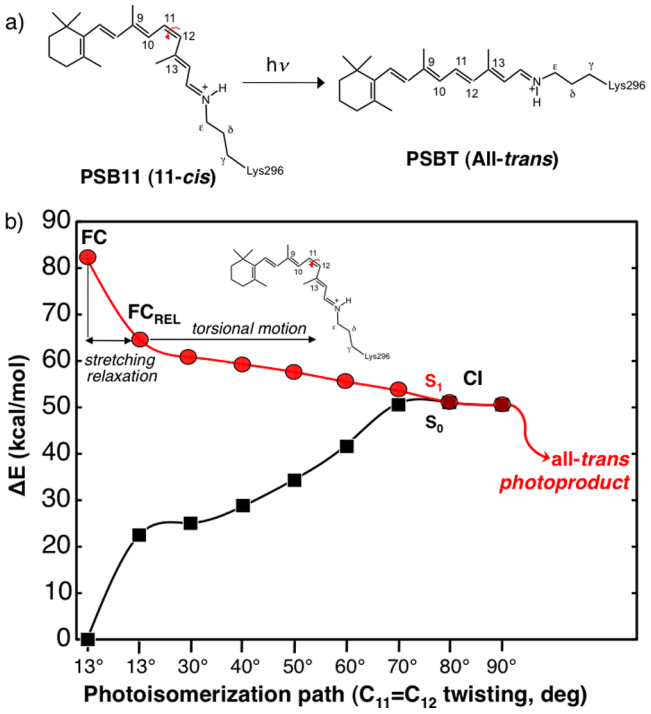

Figure 1. Schematic representation of the *cis* → *trans* photoisomerization reaction of PSB11 in rhodopsin (panel a) and the MEP calculated at the CASPT2/CASSCF level (panel b) describing the photoisomerization process from the FC point to the twisted CI funnel, through a point (FC_{REL}) where only skeletal bond stretchings have been relaxed (FC_{REL}) and subsequent structures with increasing (absolute) twisting angles.

retinals, with an avoided crossing between the S_1 and S_2 surfaces giving rise to a transition state (TS) along the S_1 state photoisomerization pathway. Indeed, the presence of an energy barrier on the S_1 energy surface before reaching the conical intersection (CI) with the ground state (GS, or S_0) would slow down the photoreaction rate and make the photoisomerization itself less efficient. In Rh on the other hand, the retinal photoisomerization occurs on a steep and barrierless reaction path involving only the ionic S_1 state and directly leading to a peaked CI, which has the form of a twisted intramolecular charge transfer (TICT) state and provides an efficient and fast (<100 fs) route for radiationless decay. According to the so-called *two-state two-mode* model,[15] skeletal deformations (namely, a bond order inversion) followed by a torsional motion of the central double bond characterize the excited state branch of the photoisomerization path.

Experimental evidence of two distinct mechanisms for retinal photoisomerization in solution and in Rh is lacking, and the available ultrafast pump−probe experiments, which are intrinsically one-dimensional (1D), do not provide sufficient data to describe the interplay between ionic and covalent states during photoisomerization. *Ad hoc* designed ultrafast nonlinear optical spectroscopy experiments are therefore needed to shed light on the retinal photoisomerization mechanisms in different environments. In order to guide the design of new time-resolved optical spectroscopy experiments, in this work, we report full characterization of the excited state manifolds of PSB11 in Rh along the retinal photoisomerization pathway. We have characterized the electronic structures of selected critical points along the minimum energy path (MEP) of the S_1 energy surface, see Figure 1b, by means of a state-of-the-art hybrid quantum mechanics (QM)/molecular mechanics (MM) approach based on wave function methods, including complete active space self-consistent field (CASSCF)[16] and second-order multireference perturbation theory (CASPT2).[17] This methodology has shown to provide consistent photophysical and photochemical data for retinals in different environments, including vacuo,[18] protein,[19] and solution,[19] in excellent agreement with chiroptical data,[20] absorption spectroscopy,[18] resonance Raman,[21] and ultrafast optical spectroscopy experiments.[22−24] A set of data collected from first-principles calculations has been used to simulate time-resolved two-dimensional (2D) electronic spectroscopy experiments of photoactivated rhodopsin. 2D electronic spectroscopy (2DES) is the ultimate third-order nonlinear optical experiment, combining high spectral and temporal resolution and providing a wealth of information which usually remains hidden in conventional pump−probe experiments, such as intra- and intermolecular electronic couplings (that are resolved as off-diagonal cross-peaks in a 2D map), pathway specific signals, homogeneous and inhomogeneous broadening, etc.[25−30] In 2DES, a sequence of three ultrashort laser pulses interacts with the sample, and the emitted signal field is detected as a function of the three time delays (t_1, t_2, and t_3); see Figure S1 in the Supporting Information. The 2D rephasing (KI) and non-rephasing (KII) signals can be obtained by double Fourier transformation (FT) with respect to times t_1 and t_3, providing 2D signals as a function of two frequencies, the "pump frequency" $\Omega(t_1)$, i.e., Ω_1, and the "probe frequency" $\Omega(t_3)$, i.e., Ω_3, given a fixed value of the "population time" t_2. For each value of the population time t_2, the 2DES spectrum can be interpreted, to a first approximation, by associating to the Ω_1 axis the absorption spectrum sensed by the excitation pulses and to the Ω_3 axis the transient absorption spectrum sensed by the probe pulse. A complete description of excited state relaxation is obtained by collecting a sequence of 2D maps as a function of population time t_2. Thus, with 2DES, the photoisomerization process of retinals can be monitored in proteins and in solution with the best possible combination of spectral and temporal resolution. Such types of experiments should be designed by setting the pump frequency resonant with ν_{max}, i.e., populating the spectroscopic state S_1, and probing the absorptions and/or the emission of the wave packet evolving on the S_1 surface with different probe frequencies and at various probe delays.

In this scenario, the unique advantage of using 2DES instead of conventional pump−probe spectroscopy is the possibility of resolving inhomogeneous broadening of the different signals along the Ω_1 axis, since there is only one diagonal peak present in the 2D map due to the $(GS)S_0 \rightarrow S_1$ transition, and off-diagonal cross-peaks are absent. Unfortunately, computational modeling of the inhomogeneous broadening of the electronic transitions requires a complete sampling of the configurational space of the ground state and the characterization of a very large number of electronic structures along the photoisomerization dynamics, which is challenging, highly computationally demanding, and beyond the scope of the present work. Nevertheless, the simulated 2DES spectra along the "static" MEP of the retinal photoisomerization can provide information on the spectral regions where signals with opposite signs, e.g., excited state absorption (ESA) versus stimulated emission (SE), overlap. In these regions, the inhomogeneous broadening of each electronic transition could significantly affect the shape of the 2D overall signal. Such an effect could be observed

dx.doi.org/10.1021/jp502538m | J. Phys. Chem. B 2014, 118, 8396−8405

experimentally, providing information on the time evolution of the 2D signals, which in conjunction with the simulated 2DES spectra reported here could give "time-resolved" atomistic details of the retinal photoisomerization reaction in Rh. Reliable characterization of temporal evolution of the electronic levels during the photoisomerization reaction requires first-principles simulations. Therefore, accurate simulations of 2DES spectra will be performed using the sum-over-states (SOS) approach,[31] as implemented in our SOS//QM/MM method,[32,33] following the evolution of the 2DES map along the photoisomerization path, otherwise not achievable with a more simple parametrized approach based on Frenkel exciton models.[32,33] Accurate simulations of the 2DES spectra have the advantage of predicting the detectable 2D signals, allowing the design of tailored experiments suited for observation of specific signals. Despite the accuracy of electronic structure calculations of the MEP points, the simulated 2DES spectra still represent a coarse picture of the experimental spectra, since here we assume that during time intervals t_1 and t_3 the electronic energy levels remain fixed, i.e., a "static" snapshot of the photoisomerizing chromophore can be recorded in an experimental 2D spectrum. To follow more precisely the evolution of the electronic excited state manifold during a real measurement, a nonadiabatic propagation of the eigenstates should be performed, but such a level of complexity is beyond the scope of this work.

Here, we focus on the detection of ESA involving low-lying covalent states of PSB11, because of their relevance in the mechanism of retinal photoisomerization. In particular, with the proposed 2DES experiments, it could be possible to detect the $S_1 \rightarrow S_2$ transitions during the photoisomerization and determine the fluctuations of the S_1/S_2 energy gap separation, elucidating the role of the low energy ionic and covalent excited states on retinal photoisomerization in Rh. A comparison between analogous 2DES experiments carried out in other proteins and in solution could finally discriminate between different photochemical mechanisms of retinal photoisomerization as a function of the (bio)chemical environment. Finally, it has been proposed that more elaborate multipulse two-dimensional techniques measuring the fifth-order nonlinear response, i.e., "transient" 2DES, could also be very informative for determining the retinal photoisomerization mechanism in different environments.[12] The electronic structure calculations and the simulations of time-resolved 2DES spectra reported here represent the groundwork for the design of such elaborate multipulse spectroscopy experiments.

THEORETICAL METHODS

Electronic Structure Calculations. Constrained geometry optimizations were performed along the $C_{10}—C_{11}=C_{12}—C_{13}$ torsion coordinate of the PSB11 ranging from −13° at FC to ca. −90° at the CI (absolute values of the twisting angle in degrees are used hereafter) were performed using a combined CASSCF(12,12)/6-31G*//Amber (QM/MM) approach and the G09 Berny-algorithm[34] through COBRAMM.[35] The QM region was described using Molpro's CASSCF routines.[36] The whole π-system of retinal and the N-terminal methylene group were considered. The β-ionone ring and its methyl groups were described by Amber99ff parameters.[22,37] QM and MM regions were connected through hydrogen link-atoms,[38] the β-ionone moiety and the two water molecules near the Schiff-base terminus were free to move during optimization, and the rest of the protein pocket was kept fixed at their crystal structure positions.[39] The ground state equilibrium structure was optimized with single state CASSCF considering only S_0, and the torsion path was obtained through state-averaging (SA) involving the S_0 and S_1 states with equal weight. SA gradients were computed using Molpro's CPMCSCF routine. As initial structures, we used optimized geometries obtained in previous work.[40] On top of the newly optimized structures, QM/MM excited state calculations were performed with Molcas 7.7[41] using the SA-CASSCF(12,12)/6-31G* method followed by energy refinement at the single-state CASPT2 level (hereafter named CASPT2/CASSCF), including all valence π-electrons and π-orbitals of the chromophore in the active space, with the MM part of the system treated as external point charges in both CASSCF and CASPT2 calculations. In the CASSCF state-averaging procedure, 70 states were included to ensure that enough roots are comprised in the CASSCF and CASPT2 calculations in order to describe the energy ranges reported for the 2D spectra. An imaginary shift[42] of 0.2 and a zero-order Hamiltonian IPEA shift of 0.0 were used. Transition dipole moments were calculated at the CASSCF level using the RASSI module of Molcas 7.7.[43]

Two-Dimensional Spectroscopy Simulations. The temporal evolution of the nonlinear response reveals electronic and geometrical changes in the system. While the recovery of the ground state bleach (B, blue arrow in Figure 2) depends on the excited state decay rates, the stimulated emission (E, cyan arrow in Figure 2) and excited state absorption (ESA, red arrows in Figure 2) exhibit characteristic shifts along the excited state deactivation pathways. In this work, we employ minimum energy path (MEP) calculations on the first excited state S_1 and probe the higher excited manifold and the ground state at selected geometries along the MEP, following the $S_1 \rightarrow S_N$ (with $N \geq 2$) and $S_1 \rightarrow S_0$ transitions at a given MEP point, respectively, while keeping the pump pulse pair in resonance with the GS $\rightarrow S_1$ transition at the Franck−Condon (FC)

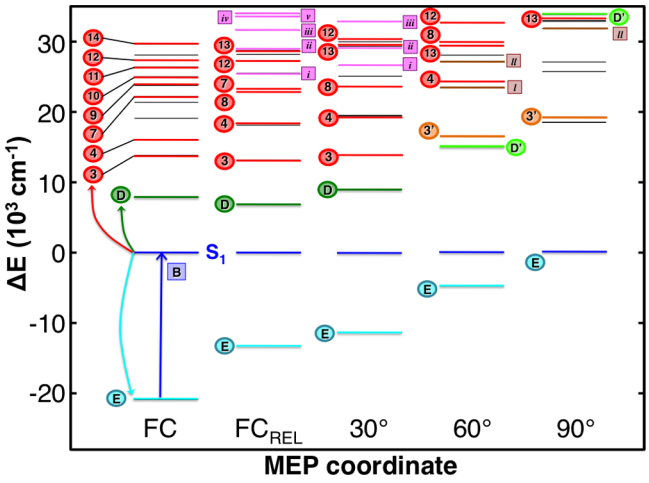

Figure 2. Evolution of the excited state manifold along the MEP of retinal photoisomerization. Selected critical points along the MEP are reported. Ground state (GS) (cyan lines), S_2 state (green lines), and high-lying excited state (bright states in red or orange and dark states in black) energies are reported using the spectroscopic S_1 state (blue lines) as zero-energy for each MEP point. Bright excited states appearing exclusively in the FC_{REL}−30° and 60−90° structures are reported with magenta and brown lines, respectively. Stimulated emission (E), GS bleaching (B), and $S_1 \rightarrow S_2$ (D and D′) transitions and excited state absorptions to higher-lying states are also depicted as arrows, only in the FC region (for simplicity).

dx.doi.org/10.1021/jp502538m | J. Phys. Chem. B 2014, 118, 8396−8405

Table 1. Excited States of the FC, FC_{REL}, 30°, 60°, and 90°(CI) Structures[a]

FC					FC_{REL}				
root	type	coeff	f	label	root	type	coeff	f	label
S1	H → L	−0.75	0.73	B	*S1*	H → L	−0.59	0.81	B
S2	D(H ⇒ L)	0.47	0.06	D	*S2*	H → L + 1	−0.40	0.27	D
						D(H ⇒ L)	−0.37		
S3	D(H, H − 1 ⇒ L)	0.37	0.11	3	*S3*	D(H, H − 1 ⇒ L)	0.40	0.07	3
	H − 3 → L	0.37				H − 2 → L	0.39		
S4	H − 1 → L	−0.51	0.68	4	*S4*	D(H, H − 2 ⇒ L)	0.39	0.05	*i*
						H − 3 → L	0.37		
S7	H − 5 → L	0.45	0.13	7	*S5*	H − 1 → L	0.54	0.59	4
S9	H → L + 1	−0.52	0.44	9	*S6*	D(H − 1 ⇒ L)	−0.38	0.08	8
S10	H − 2 → L	0.39	0.07	10	*S7*	H − 5 → L	−0.38	0.07	7
	H − 2 → L + 1	−0.36				D(H, H − 3 ⇒ L)	0.33		
S11	H − 2 → L	0.29	0.07	11	*S8*	D(H, H ⇒ L + 1)	0.26	0.24	*i*
	H − 3 → L + 1	0.24				H − 1 → L + 1	−0.25		
S12	H → L + 1	0.32	0.36	12	*S9*	H → L + 1	0.48	0.28	12
						D(H ⇒ L)	−0.34		
S14	H − 3 → L	0.33	0.14	14	*S11*	H − 4 → L	−0.61	0.04	13
					S12	H − 2 → L	0.35	0.08	*ii*
						D(H, H − 1 ⇒ L)	−0.31		
						H − 1 → L + 1	−0.31		
					S13	H − 5 → L	0.25	0.08	*iii*
						H → L + 3	0.21		
					S14	H → L + 2	0.35	0.08	*iv*
					S15	D(H − 1, H − 3 ⇒ L)	0.25	0.03	*v*
						H − 5 → L + 1	−0.19		

30°					60°				
root	type	coeff	f	label	root	type	coeff	f	label
S1	H → L	−0.59	0.73	B	*S1*	H → L	0.42	0.19	B
S2	H → L + 1	−0.42	0.32	D	*S2*	D(H, H − 1 ⇒ L)	0.54	0.13	D′
	D(H ⇒ L)	−0.33				H → L + 1	0.42		
S3	H − 2 → L	0.40	0.13	3	*S3*	H − 3 → L	0.40	0.11	3′
	D(H, H − 1 ⇒ L)	0.37				D(H, H − 1 ⇒ L)	0.36		
S4	H − 1 → L	0.55	0.65	4	*S4*	D(H, H − 3 ⇒ L)	−0.47	0.06	*l*
						H → L + 3	0.37		
S6	D(H − 1 ⇒ L)	−0.38	0.07	8	*S5*	H − 1 → L	0.66	0.62	4
	H − 2 → L	−0.35							
S8	H − 1 → L	0.25	0.17	*i*	*S6*	D(H, H − 5 ⇒ L)	0.48	0.22	*ll*
	D(H → L and H → L + 1)	0.25				H → L + 4	0.33		
S9	H − 1 → L + 1	−0.35	0.05	*ii*	*S8*	H − 4 → L	−0.52	0.07	13
	D(H, H − 1 ⇒ L)	−0.33				D(H ⇒ L, L + 1)	−0.31		
S10	H − 4 → L	0.63	0.05	13	*S9*	D(H − 1 ⇒ L)	−0.46	0.03	8
						H − 2 → L	−0.46		
S12	H → L + 1	−0.47	0.18	12	*S10*	H → L + 1	−0.48	0.29	12
S13	H − 5 → L	−0.23	0.13	*iii*					
	H − 2 → L	0.22							

90° (CI)									
root	type	coeff	f	label	root	type	coeff	f	label
S3	H − 3 → L	−0.71	0.07	3′	*S9*	H − 4 → L	−0.46	0.12	13′
	D(H, H ⇒ L + 2)	−0.39				D(H, H − 5 ⇒ L)	−0.42		
S6	D(H, H − 5 ⇒ L)	0.48	0.83	*ll*	*S10*	H → L + 1	−0.57	0.50	D′
	H − 4 → L	0.33				D(H, H − 1 ⇒ L)	0.57		

[a]Only excited states having $S_1 \rightarrow S_N$ transitions (with $N = 0, >2$) with oscillator strength (f) larger than 0.02 are reported. Electron excitations refer to active space orbitals in Figure S2 of the Supporting Information. Labels of $S_1 \rightarrow S_N$ transitions are reported for assignment of 2D peaks in Figures 2−4.

point. Evolution in the ground state is neglected; thus, the B signal arises by probing the ground state equilibrium geometry. We mainly assume that during time intervals t_1 and t_3 the electronic energy levels remain fixed, i.e., their propagation is slow with respect to the ultrafast measurement, which allows associating the electronic structure of a static MEP point with its corresponding 2D spectrum. Additional approximations are adopted: the system evolves coherently along S_1 following

dx.doi.org/10.1021/jp502538m | J. Phys. Chem. B 2014, 118, 8396−8405

closely the MEP; no population transfer between states occurs before the CI (i.e., signal intensities depend only on the transition dipole moments). It should be noted that MEP calculations do not contain dynamical and temporal information; therefore, we cannot directly extract time delays. For simulation of the 2DES spectra, we have combined the QM/MM methodology, which provides the transition dipole moments at the CASSCF level and CASPT2 corrected transition energies, with the SOS approach,[31] as implemented in our SOS//QM/MM approach documented elsewhere.[32,33] SOS calculations were performed with Spectron 2.7,[14] readapting the energy levels calculated at each MEP point in order to include the GS bleaching (GSB), i.e., by maintaining the FC S_0-S_1 energy gap and rigidly shifting all of the S_N energies calculated at the MEP point in order to align the S_1 energy with the FC S_1 energy. A constant dephasing of 200 cm^{-1} has been employed, with finite transform-limited Gaussian pulse envelopes corresponding to a bandwidth of 5000 cm^{-1}. Infinite bandwidth pulses have also been used when specified. We report the combined rephasing and nonrephasing (KI + KII) signals (hereafter named 2D signals), which have absorptive features and can be collected experimentally with either partially collinear pump−probe geometry[44,45] or heterodyne detected three-pulse photon echo configuration;[46,47] see Figure S1 in the Supporting Information. Spectra are plotted on a logarithmic scale.

RESULTS

Excited State Manifolds along the Photoisomerization Pathway. Figure 2 shows the energy levels of PSB11 along the S_1 photoisomerization MEP for energies up to 34 000 cm^{-1} (4.2 eV) from the spectroscopic state. The electronic structures calculated at the CASPT2//CASSCF level are reported from the FC region to the CI (at ∼90° twisting angle), considering a structure where only skeletal bonds have been relaxed (FC_{REL}), and two other structures with intermediate *cis* → *trans* isomerization angles, i.e., 30 and 60°. In the FC region, the first excited state accessible from the spectroscopic S_1 state is the double excitation H ⇒ L (hereafter D), i.e., the above-mentioned covalent S_2 state (see green bar in Figure 2), located at ∼8000 cm^{-1} from S_1, in agreement with previous calculations.[15] The molecular orbital labels, from H − 5 to L + 5, refer to the 12 active space orbitals in the CASSCF(12,12) calculations reported in Figure S2 in the Supporting Information. Above 10 000 cm^{-1} from S_1, the first two excited states encountered are the covalent S_3 state, characterized predominantly by double (H, H − 1 ⇒ L) and single H − 3 → L excitations, see Table 1, and the ionic S_4 state, corresponding to a single H − 1 → L excitation. The S_1 → S_2 and S_1 → $S_{3,4}$ transitions are bright (i.e., with an oscillator strength larger than 0.02, see transitions D, 3, and 4 in Figure 2) and are expected to appear in the near-infrared (NIR) and the visible (red) spectral regions, respectively. At higher energies, in the range 20 000−30 000 cm^{-1} from S_1, several excited states are found, generally characterized by single excitations into the lowest virtual orbitals (L and L + 1). In particular, the S_1 → S_7 transition (see transition 7 in Figure 2) has a transition energy close to the fundamental S_0 → S_1 transition frequency in the blue-green region of the visible spectrum, while higher-lying excited states, i.e., S_{9-12} and S_{14}, give rise to a series of ESA bands in the violet and near-UV spectral regions (see transitions 9−12 and 14 in Figure 2).

Upon photoexcitation to the spectroscopic S_1 state, the retinal chromophore undergoes skeletal relaxation[15] inducing bond order inversion and formation of a (transient) relaxed state (FC_{REL}), which is characterized by an elongated $C_{11}-C_{12}$ ("originally double") bond which allows barrier-less rotation driving the 11-*cis* → all-*trans* isomerization. As shown in Figure 2, the photoinduced skeletal relaxation induces some significant changes in the electronic structure of the chromophore. As expected, the S_0/S_1 energy gap is reduced due to the relaxation along the S_1 surface, with consequent red-shift of the S_1 → S_0 SE (hereafter E, see cyan line in Figure 2). The relative positions of the covalent S_2 and S_3 states with respect to S_1 are not significantly affected by the bond relaxation, and the corresponding transitions from S_1 result in being just slightly red-shifted with respect to FC. It is worth noting, however, that upon bond relaxation the single H → L + 1 excitation provides a significant contribution to the covalent S_2 state and the H − 2 → L excitation contributes to the S_3 state. In contrast, the skeletal relaxation induces a blue-shift of transition 4 by ∼2000 cm^{-1}. Interestingly, above 20 000 cm^{-1}, the double H − 1 ⇒ L excitation, corresponding to the S_8 state in the FC manifold (and the S_6 state in FC_{REL}), gives rise to a bright transition (transition 8) which falls in the same spectral region of transition 7 and close to the fundamental S_0 → S_1 transition frequency. Analogously, the single H − 4 → L excitation (the S_{13} state in the FC manifold and the S_{11} state in FC_{REL}) gives rise to a bright transition just below 30 000 cm^{-1} (see transition 13 in Figure 2), which, in return, is dark (i.e., with an oscillator strength smaller than 0.02) in the FC region. It is worth noting that skeletal relaxation also induces stabilization of some high-lying excited states that were not present in the FC region between 25 000 and 34 000 cm^{-1} from S_1 (see magenta lines in Figure 2, i.e., transitions *i*−*v*).

Starting from the relaxed FC_{REL} structure, the chromophore undergoes rotation about the $C_{11}-C_{12}$ bond until reaching the twisted CI, at a torsional angle of ∼90°. Here, we analyze the variations of the excited state manifold induced by this torsional motion. At 30°, we find the electronic structure of the chromophore almost unchanged with respect to the FC_{REL} structure, with a slightly less rich excited state manifold due to the disappearance of the transition 7 ESA band. All the conserved ESA bands, including transitions D, 3−4, 8, 12−13, and *i*−*iii*, are slightly blue-shifted with respect to the FC_{REL} structure, while, as expected, the SE keeps red-shifting. In contrast to the first 30° rotation, a subsequent torsion of 30° induces significant changes in the excited state manifold of the chromophore. In fact, at 60° from the FC_{REL} structure, most of the ESA bands are significantly blue-shifted (>2700 cm^{-1}) with respect to the 30° structure. Interestingly, at 60°, we observe a significant localization of the CASSCF active orbitals which significantly affects some of the ESAs. In particular, the first excited state above S_1 is now characterized mainly by the single H → L + 1 and double (H, H − 1 ⇒ L) excitations; see Table 1. The S_2 state still maintains its covalent character, but the transition from S_1 (hereafter named transition D′) blue-shifts by ∼6000 cm^{-1} with respect to the 30° structure. At 60°, the S_3 state is mainly characterized by the H − 3 → L excitation (in contrast to H − 2 → L at 30°) and the transition from S_1 (hereafter named transition 3′) is blue-shifted by ∼2750 cm^{-1} with respect to its energy at 30°, now falling nearby the D′ transition, in the red region of the visible spectrum (at ∼15 000 cm^{-1}). At energies above 20 000 cm^{-1} from S_1, excited states with mainly double excitation nature are found, see Table 1,

dx.doi.org/10.1021/jp502538m | J. Phys. Chem. B 2014, 118, 8396−8405

with corresponding bright transitions (named *I* and *II*, see brown lines in Figure 2) lying at ∼23 500 and ∼27 200 cm^{-1} and transitions 4 and 8 being blue-shifted to ∼24 300 and ∼30 000 cm^{-1}, respectively, while transition 13 remains unaffected. It should be noted that also the SE is significantly affected at 60°, red-shifting to the near-IR, well below 10 000 cm^{-1} (i.e., 1 μm). Finally, at the CI structure with a twisting angle of 90°, only a few bright transitions survive, including transitions 3′, *II*, 13, and D′. All the surviving ESA bands substantially blue-shift with respect to the 60° structure, in particular transition D′, which now lies in the near-UV at ∼33 800 cm^{-1}. Particularly at the CI, transition 3′ falls nearby the fundamental $S_0 \rightarrow S_1$ transition frequency and is expected to overlap with the GSB.

Two-Dimensional Electronic Spectra. In the above section, we have shown the changes of the electronic structure of retinal embedded in the Rh protein along the S_1 isomerization pathway, resulting in several ESA bands from S_1 to higher states, as well as an SE band from S_1 to S_0, which peak at frequencies that change very rapidly in time. Such dramatic spectral evolution of the photoinduced signals can be followed in real time using several advanced ultrafast spectroscopy techniques, such as broadband pump−probe spectroscopy or 2DES. The advantage of 2DES over pump−probe is that the nonlinear response can be resolved along the pump frequency (Ω_1), allowing characterization of cross-peaks and inhomogeneous broadenings of each electronic transition. In retinal photoisomerization there is a unique spectroscopic state (S_1) on which the photochemical reaction is known to take place. In the present work, thus, we are not interested in cross-peaks that arise from electronic coupling between different excited states (e.g., S_1−S_2, S_1−S_3 off-diagonal peaks, etc.), since their characterization requires population of higher excited states (S_2, S_3, etc.) that have unknown photophysical or photochemical pathways. We thus focus on the ESA and SE signals of the wave packet evolving only along the S_1 photoisomerization pathway. In this work, we report 2D spectra that can be experimentally collected with either the partially collinear pump−probe geometry[44,45] or the heterodyne detected three-pulse photon echo experimental setups,[46,47] using the simplest nonchiral xxxx polarization scheme.

Broadband 2D Spectra. In the previous section, we have described the evolution of the excited state manifold along the MEP of the photoisomerization, considering those excited states located below 34 000 cm^{-1} from S_1. In order to visualize the energy positions of these electronic transitions, the possible overlaps between signals and the energy shifting trends of some important transitions, we report in Figure 3 the broadband 2DES spectra calculated using all three laser pulses centered at the absorption maximum frequency of the chromophore (ν_{max}, calculated to be at 20 875 cm^{-1} at the CASPT2/CASSCF level) with infinitely broad bandwidth. Infinitely broad pulses reveal all signals that are "ideally" detectable, helping in the selection of experimental parameters (i.e., central probe frequencies and pulse bandwidths) to be used in tailored experiments for the detection of desired electronic transitions.

Figure 3 shows the broadband 2DES spectra at the FC region, i.e., at $t_2 = 0$, with the negative signals of both GSS (peak B) and SE (peak E) overlapping at Ω_3 = 20 875 cm^{-1}, i.e., the absorption maximum frequency ν_{max}, and several positive signals associated with ESA bands in the Ω_3 range from 8000 to 33 000 cm^{-1}. Following the evolution of the excited state manifolds described in the previous section, all of the 2D

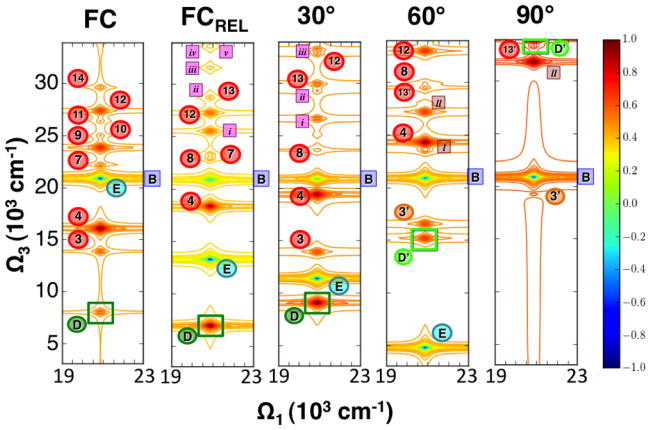

Figure 3. Broadband 2DES spectra obtained with infinitely broad laser pulses, using the xxxx nonchiral polarization scheme. 2D spectra are reported for the selected MEP point from the FC to the CI (at ∼90°). The complex part of the signal is plotted on a logarithmic scale. The transitions are labeled according to the Figure 2 assignment, with green and light green boxes highlighting the D and D′ ($S_1 \rightarrow S_2$) transitions, respectively.

signals but the GSB are expected to shift along the MEP during the photoisomerization process. The simulations of 2D spectra at $t_2 > 0$ are performed on selected geometries of the "static" MEP that cannot be directly associated with effective values of the excited state evolution time t_2. However, comparison of the reported 2DES spectra with experimental data could allow association of probe delay times with PSB11 structures, providing unprecedented atomistic details of the retinal photoisomerization.

The transition from S_1 to the covalent S_2 state (see green boxes in Figure 3, peak D) appears as a positive signal at ∼8000 cm^{-1} in the NIR at the FC region. Its transition energy does not change significantly upon skeletal relaxation (small red-shift of 1100 cm^{-1}) and 30° C_{11}−C_{12} bond rotation (blue-shift of 1000 cm^{-1} with respect to FC). A strong blue-shift of the $S_1 \rightarrow S_2$ transition is, instead, observed at a twisted angle of 60°, where the electronic excitation contributing to the covalent S_2 state changes and the corresponding ESA (peak D′) appears in the visible at ∼15 160 cm^{-1}. At the twisted CI, the S_2 state is highly destabilized and the peak D′ lies at very high energies (>30 000 cm^{-1}), in the near-UV.

The $S_1 \rightarrow S_3$ transition (peak 3) behaves similarly to the $S_1 \rightarrow S_2$ transition along the photoisomerization path. In fact, up to 30°, its transition energy is almost unchanged (between 13 100 and 13 900 cm^{-1}) with respect to its value in the FC region (i.e., 13 820 cm^{-1}), while a pronounced blue-shift of ∼2500 cm^{-1} is observed at 60°, with corresponding changes in the electronic excitations contributing to the S_3 state. Here, peak 3′ is found close to peak D′ in the red of the visible spectrum. At the CI, the $S_1 \rightarrow S_3$ transition is further blue-shifted but it lies at much lower energies than the $S_1 \rightarrow S_2$ transition, being located at ∼18 000 cm^{-1}, in proximity to the GSB (B). Indeed, the broadband 2DES spectrum at the CI reported in Figure 3 indicates that the positive peak 3′ is canceled by overlap with the strong negative B signal. It is worth noting that peak 3 disappears in the FC$_{REL}$ broadband spectrum. This is due to the progressive red-shift of the SE which bumps into low-lying ESA bands that concurrently red-shift during the photoisomerization reaction. Such a signal quenching effect is observed for the $S_1 \rightarrow S_3$ transition at the FC$_{REL}$ structure, and it is expected for the

dx.doi.org/10.1021/jp502538m | J. Phys. Chem. B 2014, 118, 8396−8405

$S_1 \rightarrow S_2$ transition at twisting angles slightly larger than 30°, i.e., ∼35°.

The $S_1 \rightarrow S_4$ transition (peak 4) is found as a positive signal at $\Omega_3 \approx 16\,000$ cm^{-1} in the FC region, and differently from peaks D and 3, it blue-shifts by ∼2100 cm^{-1} upon bond relaxations. Therefore, the overlap of (positive) peak 4 with the red-shifted (negative) SE is expected to happen at the earliest stages of the photoisomerization, i.e., during the skeletal relaxation and before the bond inversion is completed, corresponding to an energy range of 16 000−18 000 cm^{-1}. This result is fully consistent with broadband pump−probe experiments that show the absence of signals in the 16 000−18 000 cm^{-1} range (555−625 nm, in wavelength) at early probe delays, where actually the initial SE was expected to show up.[22−24] Moreover, at energies >18 000 cm^{-1}, in the spectral region of the absorption maximum ν_{max}, the experimental data at probe delays <75 fs shows the presence of a broad ESA band and its overlap with the GSB signal. Our results also indicate that, in this region of the spectra and at early probe delays (for twisting angles <60°), the negative B signal overlaps with the blue-shifting peak 4 and other two ESAs. Remarkably, at 60°, the calculated 2DES spectrum shows an almost unperturbed negative B signal and the positive peaks D′ and 3 at ∼15 200 and ∼16 500 cm^{-1}, respectively, in very nice agreement with ultrafast pump−probe spectroscopy data at around 75 fs probe delay, showing the recovery of the GSB and the appearance of positive signals at energies below 17 400 cm^{-1} (wavelengths >575 nm), with two small spots appearing at ∼16 000 and ∼16 900 cm^{-1}. Finally, our 2D spectrum at the twisted CI suggests that the only surviving bright ESA band is the $S_1 \rightarrow S_3$ transition (peak 3′), whose positive intensity is vanishing due to overlap with the negative B signal. No signals are observed below 19 000 cm^{-1}, and the first detectable ESA is in the near-UV, above 30 000 cm^{-1}, in agreement with pump−probe experiments revealing the presence of just GSB negative signal and the formation of the photoinduced ground state absorption band of the rhodopsin photoproduct in the CI region.

In summary, we showed that the broadband 2DES spectra, obtained using the excited state manifolds calculated at the CASPT2/CASSCF level along the MEP of the retinal photoisomerization, provide useful information on the evolution of ESA signals and their overlap with the SE and GSB signals with opposite sign, in good agreement with the available broadband pump−probe spectroscopy data. In the following section, we consider realistic 2DES combinations of pulse frequencies and bandwidths that can provide useful information on the evolution of specific ESA bands during retinal photoisomerization, including excitations from S_1 to low-lying covalent states that have been proposed to interplay with the spectroscopic state in the photoisomerization of retinal in solution.

One- and Two-Color 2D Spectra. The simplest 2DES combination of pulses that can be considered involves identical pump and probe pulses (*one-color* setup), with all frequencies centered at the absorption maximum of the chromophore, ν_{max}. Figure 4a shows the calculated 2DES spectra simulating such one-color experiment with the pulses' bandwidth of 5000 cm^{-1}. The major contribution to all one-color spectra is, as expected, the negative GSB signal at $\Omega_3 = \nu_{max} = 20\,875$ cm^{-1}, peak B. At the FC region, the GSB is accompanied by the SE (at identical frequency) but the simulated 2D spectrum indicates that the expected strong negative peak is partially overlapping with a positive ESA band, peak 7 at ∼22 000 cm^{-1}, inducing depletion

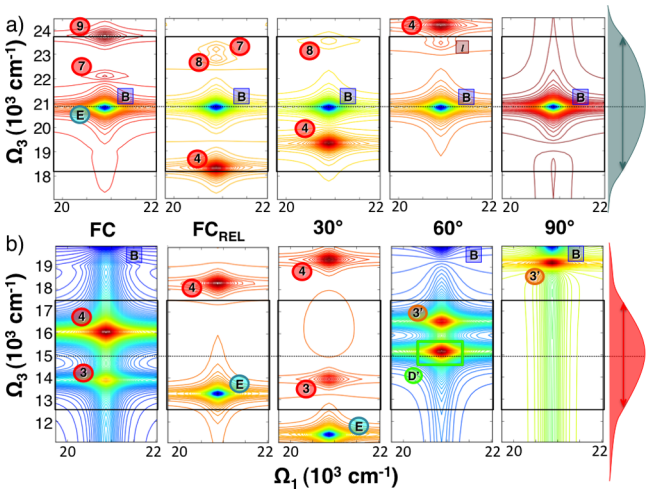

Figure 4. 2D (xxxx) spectra obtained with the *one-color* 2DVis (panel a) and the *two-color* 2DVis (panel b) setups. 2D spectra are reported for the selected MEP point from the FC to the CI (at ∼90°). The complex part of the signal is plotted on a logarithmic scale. The transitions are labeled according to the Figure 2 assignment. Black boxes indicate the 5000 cm^{-1} bandwidth that was used.

of the signal and a tiny asymmetry along the Ω_3 frequency axis. At very early probe delays, the wave packet leaves the FC region and the simulated 2DES spectra at the FC$_{REL}$ and 30° structures indicate that the negative GSB signal will be significantly depleted by a concomitant red-shift of the negative peak E, blue-shift of the positive peak 4 that is approaching ν_{max}, and lasting positive peaks 7 (at FC$_{REL}$) and 8 (at FC$_{REL}$ and 30°). At twisting angles ≥60°, the GSB signal is almost unperturbed due to the further blue-shift of the ESA band 4, which at 60° lies already at energies >24 000 cm^{-1}. At the CI, peak B almost recovers the shape of the 2D isolated signal with a tiny perturbation at energies below ν_{max} due to the presence of the blue-shifted $S_1 \rightarrow S_3$ transition. The simulated 2DES spectra along the MEP reported in Figure 4a suggest that with a one-color setup it is possible to observe modulation of the GSB signal at early stages of the photoisomerization, as affected by the evolution of high-lying ESA bands (i.e., the transitions $S_1 \rightarrow S_{4,\,7-8}$ in the FC). Probe frequencies lower than ν_{max} are necessary in order to track the energy gaps between the S_1 state and low-lying covalent excited states (such as S_2 and S_3), and a *two-color* setup is required.

Figure 4b shows the calculated 2D spectra from the FC to the CI region, simulating a time-resolved *two-color* 2DES experiment with pump pulses centered at ν_{max} ($\Omega_1 = 20\,875$ cm^{-1}) and probe pulses centered at $\Omega_3 = 15\,000$ cm^{-1}, in the red region of the visible spectrum. In the FC region, the $S_1 \rightarrow S_3$ and $S_1 \rightarrow S_4$ transitions, i.e., peaks 3 and 4, are clearly resolved at ∼13 800 and ∼16 000 cm^{-1}, respectively, but upon bond relaxation, the red-shifted SE burns the positive peak 3, while peak 4 blue-shifts to the green, at ∼18 100 cm^{-1}, and remains detectable. The positive $S_1 \rightarrow S_3$ signal will recover in the two-color spectrum upon torsional motion that further red-shifts the negative E signal. Before reaching the CI region, where the two-color 2D spectrum is essentially signal-free, the D′ transition rapidly shifts to the red and both peaks 3′ and D′ are clearly resolved at 60°. The reported two-color 2DES spectrum at 90° suggests that peak 3′ should also be resolved at the CI structure when using a probe pulse centered at 15 000 cm^{-1} with a bandwidth of 5000 cm^{-1}. The proposed *two-color*

dx.doi.org/10.1021/jp502538m | J. Phys. Chem. B 2014, 118, 8396−8405

2DES combination of pulse frequencies allows, indeed, to track the energy gaps between the S_1 state and the low-lying excited states S_{2-4} along the retinal photoisomerization pathway. However, the important $S_1 \rightarrow S_2$ transition (peak D′) appears in this detection spectral window only for twisting angles close to 60°, where the covalent S_2 state partially changes its double excitation nature (see previous section), and this transition is expected to move from ∼9000 to ∼33 000 cm^{-1} while going from 30 to 90°. Thus, the D′ signal is expected to blue-shift very rapidly from the near-IR to the UV, suggesting that it could be difficult to really track the $S_1 \rightarrow S_2$ transition with a two-color 2DES setup and detection in the visible. On the other hand, CASPT2/CASSCF calculations suggest that the position of the covalent S_2 state relative to the spectroscopic S_1 state remains almost invariant up to 30° twisting angle, with $S_1 \rightarrow S_2$ transition energies varying from 6900 to 9000 cm^{-1} in the NIR. Therefore, here we propose an alternative two-color 2D setup especially suited to track the $S_1 \rightarrow S_2$ transition during the early stage of the photoisomerization reaction, with pump pulses centered at ν_{max} and probe pulses in the NIR.

Figure 5 shows the simulated 2DES spectra for MEP structures from the FC to 60°, with NIR probe pulses centered

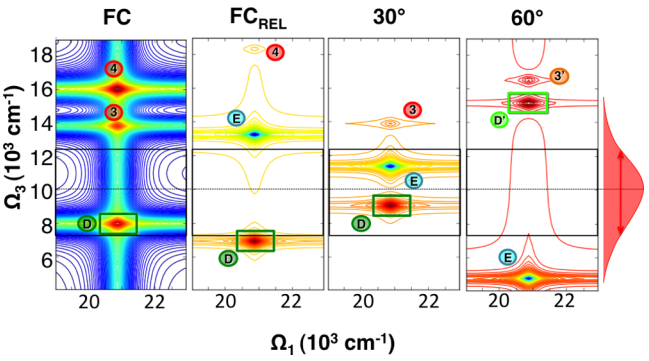

Figure 5. 2D (xxxx) spectra obtained with the *two-color* 2DVis/NIR setup. 2D spectra are reported for the selected MEP point from the FC to the 60° structure. The complex part of the signal is plotted on a logarithmic scale. The transitions are labeled according to the Figure 2 assignment. Black boxes indicate the 5000 cm^{-1} bandwidth used.

at Ω_3 = 10 000 cm^{-1} (i.e., 1 μm in wavelength) and a bandwidth of 5000 cm^{-1}, corresponding to a transform-limited pulse duration of ∼3 fs. Such tunable broadband pulses can be generated from optical parametric amplifiers.[48] With this two-color setup, peak D is clearly resolved at ∼8000, ∼6900, and ∼9000 cm^{-1}, for the FC, FC$_{REL}$, and 30° structures, respectively. In particular, both peaks E and D are near the probe central frequency at 30°, indicating that the probe frequency maximum is set very close to the region where the overlap between SE and $S_1 \rightarrow S_2$ ESA transition will occur. Unfortunately, the available pump−probe data do not cover energy values below 10 000 cm^{-1}, and direct observation of the $S_1 \rightarrow S_2$ transition at early probe delays has not been achieved yet. In the computed 2DES spectra, the evolution of the $S_1 \rightarrow S_3$ transition can also be detected from the FC to 60° structure, including its overlap with the E signal. The two-color 2DES setup with NIR probing, thus, appears to be best suited for providing a clear picture of the evolution of the $S_1 \rightarrow S_2$ and $S_1 \rightarrow S_3$ transitions, including their overlap with SE, along the retinal photoisomerization in rhodopsin.

CONCLUSIONS

In this work, we analyze the electronic structure changes of the retinal chromophore in bovine rhodopsin along its photoisomerization pathway by characterizing the manifolds of the excited states at critical points of the MEP along the S_1 energy surface, from the FC region to the twisted CI. The electronic structure calculations based on multiconfigurational *ab initio* techniques within a hybrid QM/MM scheme reveal that the S_1/S_0 energy gap rapidly decreases during the photoinduced skeletal relaxation of the polyene chain, while the evolution of excited state $S_1 \rightarrow S_N$ (with $N \geq 2$) absorption energies features a remarkable blue-shift only after bond inversion and partial rotation along the *cis* → *trans* isomerization angle, i.e., for twisting angles larger than 30°. We report simulated time-resolved 2DES spectra to track the evolution of the $S_1 \rightarrow S_0$ SE red-shift and ESA blue-shifts along the MEP. A set of broadband 2DES spectra are reported considering laser pulses with infinite bandwidth, providing a useful picture of the overall detectable 2D signals from the NIR to the near-UV frequency domains. Three different 2D combinations of pulse frequencies have been considered in order to follow the evolution of specific signals: a one-color setup with all pulses centered at the absorption maximum frequency of the chromophore in the blue-green region of the visible (one-color 2DES), a two-color setup with probe pulse centered in the red (two-color 2DVis), and a two-color setup with probe pulses centered in the NIR (two-color 2DVis/NIR). We show that a modulation of the GSB signal due to the overlap with high-lying ESA bands, i.e., transitions $S_1 \rightarrow S_{4,7-8}$, can be observed at early stages of the retinal photoisomerization using a one-color 2DVis setup. To track, instead, the energy gaps between the S_1 state and the low-lying covalent excited states (such as S_2 and S_3), a two-color setup is required. The simulated 2D spectra for the two-color 2DVis setup reveal that the signal quenching of the $S_1 \rightarrow S_3$ ESA, due to overlap with the red-shifted SE, can be detected in the red spectral window at early probe delays, while the $S_1 \rightarrow S_2$ transition is unlikely to be observed due to the large and rapid blue-shift of this signal at twisting angles larger than 30°. The $S_1 \rightarrow S_2$ transition is particularly relevant because it provides direct measurement of the S_1/S_2 energy gap separation along the photoisomerization path, a parameter that could play a crucial role in slowing down the photoreactivity, determining the photoisomerization mechanism of retinal in solution. Finally, we show that the two-color 2DVis/NIR setup is best suited for tracking the evolution of the $S_1 \rightarrow S_2$ and $S_1 \rightarrow S_3$ transitions along the retinal photoisomerization pathway, and we encourage performing such type of experiments for elucidation of the molecular mechanisms that drive different behaviors of retinal photoisomerization in various environments. The reported results are consistent with the available time-resolved 1D pump−probe experimental data, providing fundamental information for the design of new time-resolved 2D experiments and laying the groundwork for simulation of more elaborate multipulse sequences, such as in transient 2D electronic spectroscopy.

ASSOCIATED CONTENT

Supporting Information

Schematic representations of different 2DES experimental setups, CASSCF(12,12) active space orbitals, and Cartesian coordinates. This material is available free of charge via the Internet at http://pubs.acs.org.

dx.doi.org/10.1021/jp502538m | J. Phys. Chem. B 2014, 118, 8396−8405

AUTHOR INFORMATION

Corresponding Authors

*E-mail: ivan.rivalta@ens-lyon.fr. Phone: +33 04 72 72 88 43.
*E-mail: marco.garavelli@unibo.it. Phone: +39 051 20 9 9476.
*E-mail: smukamel@uci.edu.

Author Contributions

The manuscript was written through contributions of all authors. All authors have given approval to the final version of the manuscript.

Notes

The authors declare no competing financial interest.

ACKNOWLEDGMENTS

G.C. and M.G. acknowledge support by the European Research Council Advanced Grant STRATUS (ERC-2011-AdG No. 291198). S.M. gratefully acknowledges the support of the National Institute of Health Grant No. GM-59230 and the National Science Foundation through Grant No. CHE-1058791.

REFERENCES

(1) Stenkamp, R. E.; Filipek, S.; Driessen, C. A. G. G.; Teller, D. C.; Palczewski, K. Crystal Structure of Rhodopsin: A Template for Cone Visual Pigments and Other G Protein-Coupled Receptors. *Biochim. Biophys. Acta, Biomembr.* **2002**, *1565*, 168−182.

(2) Salom, D.; Lodowski, D. T.; Stenkamp, R. E.; Le Trong, I.; Golczak, M.; Jastrzebska, B.; Harris, T.; Ballesteros, J. A.; Palczewski, K. Crystal Structure of a Photoactivated Deprotonated Intermediate of Rhodopsin. *Proc. Natl. Acad. Sci. U.S.A.* **2006**, *103*, 16123−16128.

(3) Palczewski, K.; Kumasaka, T.; Hori, T.; Behnke, C. A.; Motoshima, H.; Fox, B. A.; Le Trong, I.; Teller, D. C.; Okada, T.; Stenkamp, R. E.; et al. Crystal Structure of Rhodopsin: A G Protein-Coupled Receptor. *Science* **2000**, *289*, 739−745.

(4) Li, J.; Edwards, P. C.; Burghammer, M.; Villa, C.; Schertler, G. F. X. Structure of Bovine Rhodopsin in a Trigonal Crystal Form. *J. Mol. Biol.* **2004**, *343*, 1409−1438.

(5) Nakamichi, H.; Okada, T. Local Peptide Movement in the Photoreaction Intermediate of Rhodopsin. *Proc. Natl. Acad. Sci. U.S.A.* **2006**, *103*, 12729−12734.

(6) Nakamichi, H.; Okada, T. Crystallographic Analysis of Primary Visual Photochemistry. *Angew. Chem., Int. Ed.* **2006**, *45*, 4270−4273.

(7) Choe, H. W.; Kim, Y. J.; Park, J. H.; Morizumi, T.; Pai, E. F.; Krauss, N.; Hofmann, K. P.; Scheerer, P.; Ernst, O. P. Crystal Structure of Metarhodopsin Ii. *Nature* **2011**, *471*, 651−U137.

(8) Birge, R. R. Photophysics and Molecular Electronic Applications of the Rhodopsins. *Annu. Rev. Phys. Chem.* **1990**, *41*, 683−733.

(9) Briand, J.; Bram, O.; Rehault, J.; Leonard, J.; Cannizzo, A.; Chergui, M.; Zanirato, V.; Olivucci, M.; Helbing, J.; Haacke, S. Coherent Ultrafast Torsional Motion and Isomerization of a Biomimetic Dipolar Photoswitch. *Phys. Chem. Chem. Phys.* **2010**, *12*, 3178−3187.

(10) Lumento, F.; Zanirato, V.; Fusi, S.; Busi, E.; Latterini, L.; Elisei, F.; Sinicropi, A.; Andruniow, T.; Ferre, N.; Basosi, R.; et al. Quantum Chemical Modeling and Preparation of a Biomimetic Photochemical Switch. *Angew. Chem., Int. Ed.* **2007**, *46*, 414−420.

(11) Baylor, D. How Photons Start Vision. *Proc. Natl. Acad. Sci. U.S.A.* **1996**, *93*, 560−565.

(12) Rivalta, I.; Nenov, A.; Garavelli, M. Modelling Retinal Chromophores Photoisomerization: From Minimal Models in Vacuo to Ultimate Bidimensional Spectroscopy in Rhodopsins. *Phys. Chem. Chem. Phys.* **2014**, DOI: 10.1039/c3cp55211j.

(13) Schulten, K.; Humphrey, W.; Logunov, I.; Sheves, M.; Xu, D. Molecular Dynamics Studies of Bacteriorhodopsin's Photocycles. *Isr. J. Chem.* **1995**, *35*, 447−464.

(14) Gai, F.; Hasson, K. C.; McDonald, J. C.; Anfinrud, P. A. Chemical Dynamics in Proteins: The Photoisomerization of Retinal in Bacteriorhodopsin. *Science* **1998**, *279*, 1886−1891.

(15) Gonzalez-Luque, R.; Garavelli, M.; Bernardi, F.; Merchan, M.; Robb, M. A.; Olivucci, M. Computational Evidence in Favor of a Two-State, Two-Mode Model of the Retinal Chromophore Photoisomerization. *Proc. Natl. Acad. Sci. U.S.A.* **2000**, *97*, 9379−9384.

(16) Roos, B. O. *Ab Initio Methods in Quantum Chemistry: Part II*; Wiley: Chichester, U.K., 1987.

(17) Andersson, K.; Malmqvist, P. A.; Roos, B. O. 2nd-Order Perturbation-Theory with a Complete Active Space Self-Consistent Field Reference Function. *J. Chem. Phys.* **1992**, *96*, 1218−1226.

(18) Rajput, J.; Rahbek, D. B.; Andersen, L. H.; Hirshfeld, A.; Sheves, M.; Altoe, P.; Orlandi, G.; Garavelli, M. Probing and Modeling the Absorption of Retinal Protein Chromophores in Vacuo. *Angew. Chem., Int. Ed.* **2010**, *49*, 1790−1793.

(19) Altoe, P.; Stenta, M.; Bottoni, A.; Garavelli, M. A Tunable Qm/Mm Approach to Chemical Reactivity, Structure and Physico-Chemical Properties Prediction. *Theor. Chem. Acc.* **2007**, *118*, 219−240.

(20) Buss, V.; Kolster, K.; Terstegen, F.; Vahrenhorst, R. Absolute Sense of Twist of the C12-C13 Bond of the Retinal Chromophore in Rhodopsin-Semiempirical and Nonempirical Calculations of Chiroptical Data. *Angew. Chem., Int. Ed.* **1998**, *37*, 1893−1895.

(21) Garavelli, M.; Negri, F.; Olivucci, M. Initial Excited-State Relaxation of the Isolated 11-Cis Protonated Schiff Base of Retinal: Evidence for in-Plane Motion from Ab Initio Quantum Chemical Simulation of the Resonance Raman Spectrum. *J. Am. Chem. Soc.* **1999**, *121*, 1023−1029.

(22) Polli, D.; Altoe, P.; Weingart, O.; Spillane, K. M.; Manzoni, C.; Brida, D.; Tomasello, G.; Orlandi, G.; Kukura, P.; Mathies, R. A.; et al. Conical Intersection Dynamics of the Primary Photoisomerization Event in Vision. *Nature* **2010**, *467*, 440−U88.

(23) Peteanu, L. A.; Schoenlein, R. W.; Wang, Q.; Mathies, R. A.; Shank, C. V. The 1st Step in Vision Occurs in Femtoseconds - Complete Blue and Red Spectral Studies. *Proc. Natl. Acad. Sci. U.S.A.* **1993**, *90*, 11762−11766.

(24) Schoenlein, R. W.; Peteanu, L. A.; Mathies, R. A.; Shank, C. V. The 1st Step in Vision - Femtosecond Isomerization of Rhodopsin. *Science* **1991**, *254*, 412−415.

(25) Mukamel, S. *Principles of Nonlinear Optical Spectroscopy*; Oxford University Press: New York, 1995.

(26) Hamm, P.; Zanni, M. *Concepts and Methods of 2d Infrared Spectroscopy*; Cambridge University Press: Cambridge, U.K., 2011.

(27) Zhuang, W.; Hayashi, T.; Mukamel, S. Coherent Multidimensional Vibrational Spectroscopy of Biomolecules: Concepts, Simulations, and Challenges. *Angew. Chem., Int. Ed.* **2009**, *48*, 3750−3781.

(28) Zanni, M. T.; Hochstrasser, R. M. Two-Dimensional Infrared Spectroscopy: A Promising New Method for the Time Resolution of Structures. *Curr. Opin. Struct. Biol.* **2001**, *11*, 516−522.

(29) Mukamel, S. Multidimensional Femtosecond Correlation Spectroscopies of Electronic and Vibrational Excitations. *Annu. Rev. Phys. Chem.* **2000**, *51*, 691−729.

(30) West, B. A.; Moran, A. M. Two-Dimensional Electronic Spectroscopy in the Ultraviolet Wavelength Range. *J. Phys. Chem. Lett.* **2012**, *3*, 2575−2581.

(31) Chen, G. H.; Mukamel, S.; Beljonne, D.; Bredas, J. L. The Coupled Electronic Oscillators Vs the Sum-over-States Pictures for the Optical Response of Octatetraene. *J. Chem. Phys.* **1996**, *104*, 5406−5414.

(32) Rivalta, I.; Nenov, A.; Cerullo, G.; Mukamel, S.; Garavelli, M. Ab Initio Simulations of Two-Dimensional Electronic Spectra: The Sos//Qm/Mm Approach. *Int. J. Quantum Chem.* **2014**, *114*, 85−93.

(33) Nenov, A.; Rivalta, I.; Cerullo, G.; Mukamel, S.; Garavelli, M. Disentangling Peptide Configurations Via Two-Dimensional Electronic Spectroscopy: Ab Initio Simulations Beyond the Frenkel Exciton Hamiltonian. *J. Phys. Chem. Lett.* **2014**, *5*, 767−771.

(34) Frisch, M. J.; Trucks, G. W.; Schlegel, H. B.; Scuseria, G. E.; Robb, M. A.; Cheeseman, J. R.; Scalmani, G.; Barone, V.; Mennucci,

B.; Petersson, G. A.; et al. *Gaussian 09*, revision A.1; Gaussian, Inc.: Wallingford, CT, USA, 2009.
(35) Altoe, P.; Stenta, M.; Bottoni, A.; Garavelli, M., Cobramm: A Tunable Qm/Mm Approach to Complex Molecular Architectures. Modelling the Excited and Ground State Properties of Sized Molecular Systems. In *Computational Methods in Science and Engineering Vol 1: Theory and Computation: Old Problems and New Challenges*; Maroulis, G., Simos, T. E., Eds.; American Institute of Physics: Melville, NY, 2007; Vol. *963*, pp 491−505.
(36) Werner, H. J.; Knowles, P. J.; Knizia, G.; Manby, F. R.; Schutz, M. Molpro: A General-Purpose Quantum Chemistry Program Package. *Wiley Interdiscip. Rev.: Comput. Mol. Sci.* **2012**, *2*, 242−253.
(37) Case, D. A.; Cheatham, T. E.; Darden, T.; Gohlke, H.; Luo, R.; Merz, K. M.; Onufriev, A.; Simmerling, C.; Wang, B.; Woods, R. J. The Amber Biomolecular Simulation Programs. *J. Comput. Chem.* **2005**, *26*, 1668−1688.
(38) Senn, H. M.; Thiel, W. Qm/Mm Methods for Biomolecular Systems. *Angew. Chem., Int. Ed.* **2009**, *48*, 1198−1229.
(39) Okada, T.; Sugihara, M.; Bondar, A. N.; Elstner, M.; Entel, P.; Buss, V. The Retinal Conformation and Its Environment in Rhodopsin in Light of a New 2.2 Angstrom Crystal Structure. *J. Mol. Biol.* **2004**, *342*, 571−583.
(40) Tomasello, G.; Olaso-Gonzalez, G.; Altoe, P.; Stenta, M.; Serrano-Andres, L.; Merchan, M.; Orlandi, G.; Bottoni, A.; Garavelli, M. Electrostatic Control of the Photoisomerization Efficiency and Optical Properties in Visual Pigments: On the Role of Counterion Quenching. *J. Am. Chem. Soc.* **2009**, *131*, 5172−5186.
(41) Aquilante, F.; De Vico, L.; Ferre, N.; Ghigo, G.; Malmqvist, P. A.; Neograd y, P.; Pedersen, T. B.; Pitonak, M.; Reiher, M.; Roos, B. O.; et al. Software News and Update Molcas 7: The Next Generation. *J. Comput. Chem.* **2010**, *31*, 224−247.
(42) Forsberg, N.; Malmqvist, P. A. Multiconfiguration Perturbation Theory with Imaginary Level Shift. *Chem. Phys. Lett.* **1997**, *274*, 196−204.
(43) Malmqvist, P. A.; Roos, B. O. The Casscf State Interaction Method. *Chem. Phys. Lett.* **1989**, *155*, 189−194.
(44) Tian, P. F.; Keusters, D.; Suzaki, Y.; Warren, W. S. Femtosecond Phase-Coherent Two-Dimensional Spectroscopy. *Science* **2003**, *300*, 1553−1555.
(45) Grumstrup, E. M.; Shim, S.-H.; Montgomery, M. A.; Damrauer, N. H.; Zanni, M. T. Facile Collection of Two-Dimensional Electronic Spectra Using Femtosecond Pulse-Shaping Technology. *Opt. Express* **2007**, *15*, 16681−16689.
(46) Brixner, T.; Stiopkin, I. V.; Fleming, G. R. Tunable Two-Dimensional Femtosecond Spectroscopy. *Opt. Lett.* **2004**, *29*, 884−886.
(47) Cowan, M. L.; Ogilvie, J. P.; Miller, R. J. D. Two-Dimensional Spectroscopy Using Diffractive Optics Based Phased-Locked Photon Echoes. *Chem. Phys. Lett.* **2004**, *386*, 184−189.
(48) Brida, D.; Manzoni, C.; Cirmi, G.; Marangoni, M.; Bonora, S.; Villoresi, P.; De Silvestri, S.; Cerullo, G. Few-Optical-Cycle Pulses Tunable from the Visible to the Mid-Infrared by Optical Parametric Amplifiers. *J. Opt.* **2010**, *12*.